Nanoparticles for Stem Cells

DOI: 10.1002/ange.201302245

Multimodal Magnetic Core–Shell Nanoparticles for Effective Stem-Cell Differentiation and Imaging**

*Birju Shah, Perry T. Yin, Shraboni Ghoshal, and Ki-Bum Lee**

Stem cells, owing to their ability to differentiate into specialized cells that can serve a particular function, have enormous potential in the field of regenerative medicine, wherein these stem-cell-based therapies can be used to treat a wide range of diseases including diabetes, heart disease, and liver disease.[1] However, the realization of stem-cell-based therapies in the clinic is severely hampered by our current inability to achieve the efficient delivery of genetic materials into target cells, which is required to specifically direct differentiation. In particular, with regard to stem-cell-based regenerative medicine, it is vital to achieve: 1) the highly efficient transfection of targeted cells, 2) biocompatibility, with an emphasis on maintaining a high cell viability without altering migratory and differentiation potential, and 3) non-invasive monitoring for the long-term evaluation of therapy.[2]

Currently, the use of virus-mediated delivery results in the highest delivery efficiency (80–90%) for stem cells.[3] However, this method also has a number of harmful effects that limit its clinical applicability, including potential cell toxicity, mutagenesis, and the induction of an immune response.[4] To this end, a significant amount of effort has been invested in the development of alternative non-viral delivery methods.[2c] In particular, recent studies have demonstrated that magnetic nanoparticles (MNPs) possess a number of advantages that are especially attractive for application to stem cell research.[5] Typically, MNPs are composed of a magnetic core that can consist of metals or metal oxides,[6] metal alloys,[7] and, more recently, doped metals.[8] These MNP cores can then be post-synthetically modified with a biocompatible material (for example, SiO_2, gold, polymer) resulting in a core–shell structure.[9] In doing so, this shell can not only act as a hydrophilic layer, but also as a platform for the surface functionalization of the MNPs.[10] As a result of its inherent magnetism, the properties of the shell, and the surface functionalization employed, MNPs can possess multifunctionalities including the delivery of nucleic acids such as plasmid DNA (pDNA) and short interfering RNA (siRNA), magnetically facilitated delivery, cell targeting, and MRI contrast agents.[11] In particular, the synthesis of gold-coated MNPs can provide a number of additional advantages, such as near-infrared (NIR) absorption,[12] photon scattering, and a relatively inert and facile surface that is amenable to further functionalization, while preserving the core magnetic properties.[13]

Herein, we describe the synthesis of well-defined magnetic core–shell nanoparticles (MCNPs), composed of a highly magnetic core surrounded by a thin uniform gold shell, and their application for the delivery of genetic materials (siRNA and pDNA) into stem cells in a highly efficient, spatiotemporally controlled, and biocompatible manner (Figure 1). Moreover, we demonstrate the utility of the various functions that are provided by our MCNP system, including magnetically facilitated transfection and dark-field imaging. Although numerous studies have previously utilized

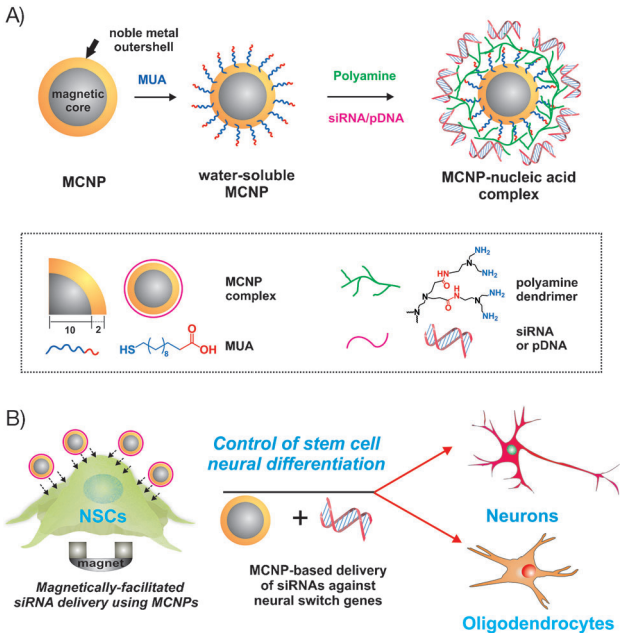

Figure 1. Synthesis of NPs and their application for the differentiation of stem cells. A) Generation of non-water-soluble MCNPs and water-soluble MCNPs. B) Magnetically facilitated siRNA delivery using MCNPs to control the differentiation of stem cells.

[*] B. Shah, S. Ghoshal, Prof. K.-B. Lee
Department of Chemistry & Chemical Biology, Institute for Advanced Materials, Devices and Nanotechnology (IAMDN), Rutgers, The State University of New Jersey
Piscataway, NJ 08854 (USA)
E-mail: kblee@rutgers.edu
Homepage: http://rutchem.rutgers.edu/~kbleeweb/
P. T. Yin
Department of Biomedical Engineering, Rutgers, The State University of New Jersey, Piscataway, NJ 08854 (USA)

[**] This work was financially supported by the NIH Director's Innovator Award [(1DP20D006462-01), K.B.L.] and a N.J. Commission on Spinal Cord grant [(09-3085-SCR-E-0), K.B.L.]. P.T.Y. would like to acknowledge NIH Biotechnology Training Grant for support. We would like to thank Prasad Subramaniam and Nicholas Pasquale for their useful comments on the manuscript.

Supporting information for this article, including experimental details and methods, is available on the WWW under http://dx.doi.org/10.1002/anie.201302245.

MNPs as MRI contrast agents and have shown the effectiveness of magnetically facilitated transfection in stem cells, the use of MCNPs to mediate the delivery of genetic materials to stem cells in a highly efficient and biocompatible manner remains to be assessed. To this end, as a proof-of-concept experiment for the genetic manipulation of stem cells using MCNPs and the accompanying differentiation studies, neural stem cells (NSCs) were chosen, as they are known to be very sensitive to conventional exogenous lipid-based transfection reagents, as well as difficult to transfect.[2a] Specifically, we hypothesized that we could achieve a significantly higher transfection efficiency for genetic materials without compromising stem cell viability and biological functions (such as differentiation) using our MCNP-based magnetically facilitated delivery. Moreover, we hypothesized that the gold shell would provide additional advantages for stem-cell-based therapies through the ability to perform dark-field imaging, as this would be a simple method with which to confirm the presence of MCNPs within stem cells prior to transplantation or other studies.

For the formation of our MCNPs, we chose doped magnetic nanoparticles ($ZnFe_2O_4$) as our core, as these MNPs have been shown to have a significantly higher magnetic susceptibility and hence can afford improved magnetic properties at much lower concentrations when compared to conventional MNPs.[8] As such, we first synthesized these $ZnFe_2O_4$ NPs by the thermal decomposition of a mixture of metal precursors in the presence of oleic acid as a stabilizer, using a modified version of a previously reported method.[8] These $ZnFe_2O_4$ NPs were then coated with a thin layer of Au by reducing hydrogen tetrachloroaurate hydrate ($HAuCl_4 \cdot 3H_2O$) in a chloroform solution of oleylamine in the presence of $ZnFe_2O_4$ NPs, which resulted in the formation of non-water-soluble MCNPs (Figure 1A).[14] These non-water-soluble $ZnFe_2O_4$@Au nanoparticles were then rendered water-soluble by exchanging their surface oleylamine moieties with 11-mercaptoundecanoic acid (MUA).[15] Initial characterization was performed to confirm that the water-soluble MCNPs (Figure 1A) retained their magnetic properties (Figure 2D) and showed a distinct pink coloration, which resembles a gold colloidal solution (Figure 2E), owing to the surface plasmon resonance (SPR) properties of the outer Au shell.

A detailed characterization of the $ZnFe_2O_4$@Au NPs was then performed. First, transmission electron microscopy (TEM) analysis revealed that the overall diameter increased from 20 ± 1.2 nm ($n = 100$) for the $ZnFe_2O_4$ MNPs (Supporting Information, Figure S1) to 25 ± 2.7 nm ($n = 100$; Figure 2A). The lattice fringes in the Au shell can clearly be seen in the HRTEM (Figure 2B), and the interfringe spacing was found to be 0.201 nm, which is the interplane distance of the (200) planes in the face centered cubic (fcc) Au. This indicates that the $ZnFe_2O_4$ nanoparticles are indeed coated with a layer of crystalline Au (ca. 2.5 nm). Furthermore, from the HRTEM images (Figure 2B), we observed a difference in the contrast between the darker $ZnFe_2O_4$ core and the lighter Au shell. It has been reported that this is attributed to the dominance of the mass contrast over the diffraction contrast, making Au appear lighter in spite of it having a higher

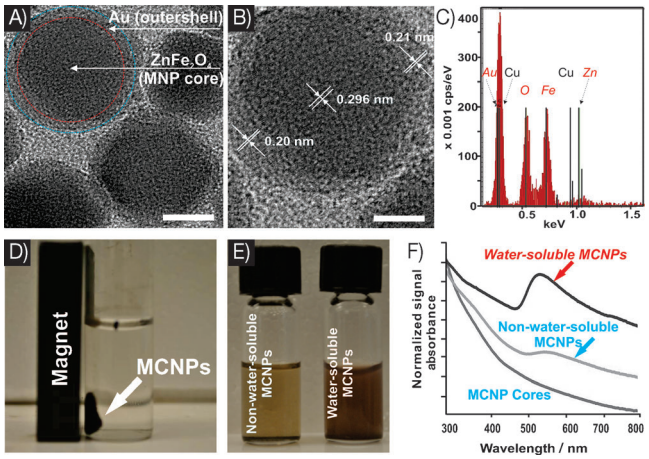

Figure 2. A) TEM image of the MCNPs. Scale bar = 10 nm, B) HRTEM image of a single MCNP. Scale bar = 5 nm, C) EDAX spectra of individual MCNPs, D) Representative picture showing that the MCNPs dispersed in water are attracted to a magnet. E) Representative picture of non-water-soluble and water-soluble MCNPs in solution. The light pink color of water-soluble MCNPs indicates the formation of a gold shell. F) UV/Vis absorption spectra of the MCNP cores, non-water-soluble MCNPs and water-soluble MCNPs. The cores and non-water-soluble MCNPs were dissolved in chloroform before UV/Vis analysis.

electron density than Fe and Zn.[16] We also confirmed that the MCNPs were composed of Zn, Fe, and Au using energy dispersive X-ray spectroscopy (EDAX) analysis (Figure 2C). Finally, from the UV absorption data (Figure 2F), we clearly observed that the water-soluble MCNPs show a distinct absorption peak at 540 nm, because of the SPR properties of the water-soluble Au nanostructures. As expected, this peak is not observed in the core $ZnFe_2O_4$ MNPs or the non-water-soluble $ZnFe_2O_4$@Au NPs coated with oleylamine.

To prepare these aforementioned MCNP constructs for the delivery of functional genetic material such as siRNA or plasmid DNA (pDNA), the water-soluble MCNPs were coated with a cationic polyamine dendrimer that was previously developed by our group[17] (Figure 1A; see also Figure S2) to afford an overall positive charge to the MCNPs. This positive charge facilitated MCNP complexation with negatively charged siRNA or pDNA. Furthermore, the cationic polyamine dendrimer has multiple primary amine groups and hence, once the MCNP constructs are internalized, it can act as a proton sponge in the endosomes, thereby aiding in subsequent endosomal escape of the complexes and protecting the cargo from the deleterious effects of the acidic microenvironment.[17] The hydrodynamic size of the final MCNP constructs was determined to be 70 ± 2 nm and their net surface charge was found to be $+15$ mV using dynamic light scattering (DLS) and zeta potential measurements, respectively (Figure S3). Additionally, we determined the amount of siRNA bound to the positively charged MCNPs at different concentrations using a Picogreen assay (Figure S4).

Once we finished optimizing the synthesis of the MCNP constructs, we tested whether the MCNPs, and/or the use of magnetically facilitated delivery, negatively affects the intrinsic ability of NSCs to proliferate and differentiate. To accomplish this, we used immunocytochemistry to assess the

proliferation and differentiation capabilities of the NSCs following their exposure to increasing concentrations of MCNPs (2–20 $\mu g\,mL^{-1}$; Figure S5) that are complexed with negative control siRNA either in the presence or absence of an external magnetic field (MF). Based on the expression of proliferation (Ki67) and differentiation (TUJ1 for neurons and GFAP for glial cells) markers, we were able to ascertain that the intrinsic biological functions of the NSCs were unaffected by our MCNPs and the delivery methods employed (Figure 3A). As we had confirmed the excellent biocompatibility and non-toxicity of our MCNPs in NSCs, we went ahead and tested the capability of these MCNPs to translocate genetic material (siRNA or pDNA) into NSCs-GFP, which are genetically labeled with green fluorescent protein (GFP), in the presence or absence of an external MF and compared to commercially available transfection agents such as X-tremeGENE. To this end, we first identified the optimal external MF exposure time that results in maximum transfection efficiency while preventing deleterious effects to cell viability (Figure S6). To accomplish this, we complexed the MCNPs with Cy3-labeled control siRNA (red color, Silencer, Ambion) and incubated these complexes with NSCs-GFP in the presence of a MF for increasing periods of time ranging from 0 to 6 h. After each exposure time point, the NSCs-GFP were washed with Dulbecco's phosphate-buffered saline (DPBS) three times to remove untransfected MCNP-siRNA constructs. Using fluorescence microscopy, we observed a sharp increase in the uptake and localization of the tested MCNP-siRNA constructs (Figure 3B) into the cytoplasm of the NSCs-GFP after the complexes were incubated with the NSCs for only 30 min in the presence of a MF, as compared to control (Figure 3B). Upon increasing the time of incubation, we observed a minimal increase in the uptake and localization of MCNP-siRNA constructs (Figure S7). As such, we subsequently identified 30 min as the optimum MF exposure time to offset any deleterious effects to the NSCs-GFP and used this for all of the following experiments.

Next, to demonstrate the delivery of functional MCNP-siRNA constructs, we chose siRNA against GFP (siGFP) and optimized the concentrations of MCNP and siGFP to be delivered by varying their respective concentrations and measuring the resulting GFP knockdown efficiency (Figure S8). Once we identified the optimum concentrations of MCNP (5 $\mu g\,mL^{-1}$) and siGFP (200 nM), we compared the knockdown efficiency of MCNP-based trasfection with that of the commercial transfection agent, X-tremeGENE. Specifically, the X-tremeGENE was complexed with the same concentration of siRNA (200 nM) in a ratio of 3:1, as recommended by the manufacturer. To this end, the MCNP–siGFP and X-tremeGENE–siGFP constructs were incubated with NSCs-GFP for periods of time increasing from 15 min to 6 h, to first elucidate the correlation between the incubation time and the transfection efficiency, wherein we used the optimized MF exposure time (30 min) for all conditions. For comparison, we used the recommended incubation time (6 h) for X-tremeGENE. After each period of incubation, the cells were washed with DPBS three times and further incubated for a period of 72 h, following which we

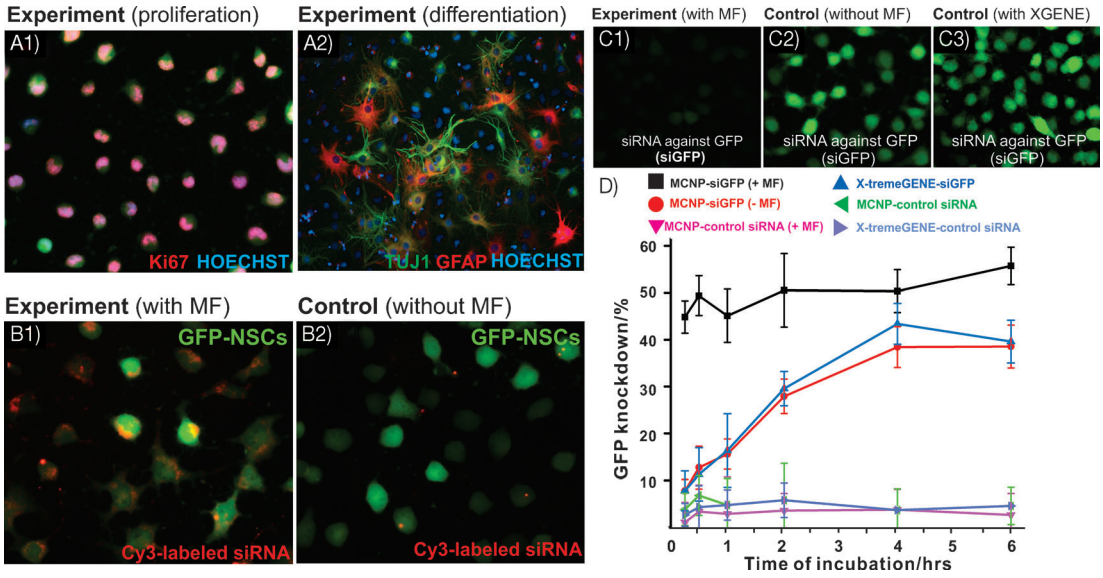

Figure 3. A) Immunostaining data showing the proliferation (A1) and differentiation (A2) capability of NSCs after treatment with MCNPs (MCNPs, 5 $\mu g\,mL^{-1}$; negative control siRNA, 200 nM) in the presence of a magnetic field (MF). The NSCs were stained with Ki67 as a proliferation marker and with TUJ1 (neurons) and GFAP (astrocytes) as differentiation markers. The nucleus was stained with Hoechst stain. B) Effects of the presence (B1) and absence (B2) of MF on the uptake of MCNP–Cy-3 labeled siRNA (MCNPs, 5 $\mu g\,mL^{-1}$; Cy-3 labeled siRNA, 200 nM) complexes in the NSCs. C) Knockdown of GFP fluorescence signal in NSCs treated with MCNPs- siGFP complexes in the presence (C1) or absence (C2) of an external magnetic field. The knockdown efficiency using MCNPs was compared to that using X-TremeGENE (C3) as a positive control. The concentrations of MCNPs and siGFP were 5 $\mu g\,mL^{-1}$ and 200 nM respectively. The amount of X-TremeGENE used was within the manufacturer-recommended range. The cells were exposed to the magnetic field for an optimum period of 30 min. D) Quantification of time-dependent GFP knockdown efficiency in NSCs using MCNPs (with or without magnetic field) and X-TremeGENE complexed with either siGFP or control siRNA. As described in (C), the concentrations of MCNPs and siGFP were 5 $\mu g\,mL^{-1}$ and 200 nM, respectively.

quantified the decrease in the GFP signal intensity of the NSCs. We saw a significant difference in the gene silencing capability of MCNPs in the presence of a MF (55.45% knockdown, $p < 0.01$) as compared to that in the absence of a MF (36.75% knockdown; Figure 3C), when the complexes were incubated for 6 h. Moreover, upon comparison of our magnetically-facilitated delivery with X-tremeGENE-based delivery, we observed a remarkable difference in the time-dependent progression curve of the transfection efficiency (Figure 3D) and in the cytotoxic effects exhibited by the two experimental conditions (Figure S9). In the case of magnetically facilitated delivery (MCNP–siGFP/MF, Figure 3D), significantly higher levels of GFP knockdown (45.6% knockdown, $p < 0.01$) were observed after only 15 min of incubation with negligible cytotoxicity (ca. 97% cell viability; see also Figure S9). Moreover, an additional increase in gene silencing was seen after increasing the incubation time to 6 h (55.45% knockdown). In contrast, negligible GFP knockdown was seen in the case of X-tremeGENE–siGFP complexes after 15 min of incubation, which gradually increased upon increasing the incubation time, and reached a plateau (38.95% knockdown, Figure 3D) after 6 h; however, with significant cytotoxicity (60% cell viability, $p < 0.01$; Figure S9). From the analysis of the GFP knockdown results (Figure 3D), we identified 30 min as the optimum incubation period needed to achieve significant downstream effects from gene delivery using MCNP/MF.

To see whether we could further increase transfection efficiency, we carried out repeated transfections of the same cell culture, a technique known as multifection,[18] using our MCNP/siGFP constructs and compared the gene-silencing efficiency achieved with multifection to that of a single transfection. We found that we were able to further improve the gene silencing efficiency from 55% (single transfection of MCNP/siGFP) to 65% (multifection of MCNP/siGFP; Figure S10a). In the case of X-tremeGENE multifection, we observed a similar trend of increased GFP knockdown (45% for multifection vs. 38% for single transfection). However, upon comparing their toxicity profiles, the viability of cells multi-transfected with MCNPs only decreased slightly ($p > 0.05$ vs. control), whereas that of X-tremeGENE resulted in significant cell death ($p < 0.01$ vs. control; Figure S10b). Finally, besides siRNA, we also demonstrated the delivery of plasmid DNA, DsRED, a red fluorescent protein from Discosoma sp., to NSCs–GFP using our MCNPs under similar experimental conditions to siRNA delivery. The magnetically facilitated delivery of MCNP–DsRED complexes led to significantly higher levels of gene expression in NSCs within a shorter incubation time than the same complexes in the absence of a MF (Figure S11). Thus, we observed that, in spite of shorter than commonly used incubation times, highly efficient gene deactivation (in the case of siGFP; Figure 3) or activation (in the case of DsRED; Figure S11) was achieved with negligible toxicity when magnetically facilitated delivery of MCNP constructs was utilized. This is in contrast to that seen with the positive control experiments using standard transfection agents under the same conditions. However, to achieve comparable levels of knock-down results using the aforementioned lipid-based transfection methods, we typically needed longer incubation times (> 6 h), which can induce significant cytotoxic effects, resulting in a low cell viability (ca. 60% cell viability).

Having demonstrated that our MCNPs, in the presence of a MF, can efficiently manipulate gene expression in NSCs without compromising their biological functions, we focused on controlling the neural differentiation of NSCs using our optimized conditions (Figure 4A) to demonstrate the utility of our MCNPs for stem-cell-based therapies. For this demonstration, we selected functional siRNAs targeting the key genes *CAVEOLIN-1* (si*CAV*)[19] and *SOX9* (si*SOX9*)[20] (Figure 4A). These two genes have already been identified as "neural switches" that, when inhibited, selectively control the differentiation of NSCs into oligodendrocytes and neurons, respectively. To demonstrate the effective genetic manipulation of NSCs to control their differentiation, the MCNP–siRNA complexes (MCNP, 5 μg mL^{-1}; si*CAV*/si*SOX9*,

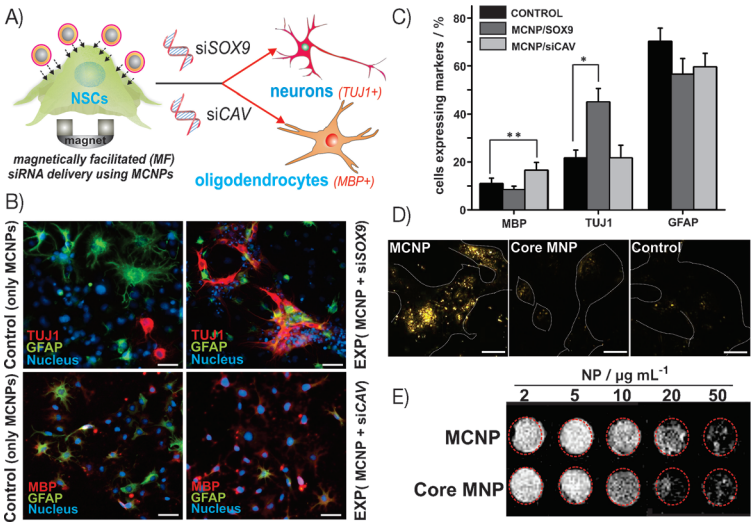

Figure 4. A) MCNP-mediated magnetically facilitated delivery of siRNA against *SOX9* (si*SOX9*) and *CAVEOLIN-1* (si*CAV*) for inducing neural differentiation of NSCs. B) Fluorescence microscopy images depicting neuronal (top row) and oligodendrocyte differentiation (bottom row) of the NSCs following delivery of si*SOX9* and si*CAV*, respectively, using MCNPs. The NSCs were stained with MBP (oligodendrocytes) and GFAP (astrocytes) in the case of MCNP/si*CAV*-treated cells and for TUJ1 (neurons) and GFAP (astrocytes) in case of MCNP/si*SOX9*-treated cells on day 7 of transfection. The nucleus was stained with Hoechst stain. Scale bar = 1 μm. C) Quantification of percent cells expressing neural markers when treated MCNP/siCAV and MCNP/siSOX9 versus untreated cells. All results represent the average mean of three independent experiments. Values are represented as mean ± SD. An asterisk (*) denotes $p < 0.001$ for neuronal differentiation and a double asterisk (**) denotes $p < 0.01$ for oligodendrocyte differentiation. D) Dark-field light-scattering images for NSCs treated with MCNPs, Core ($ZnFe_2O_4$) MNPs and untreated NSCs (control). The dark-field scattering signals in the core MNP and the control experiments come from the background signals of cellular components. Scale bar is 100 nm. E) Signal-intensity T2-weighted MR images of MCNP and core NPs in phantom agar gel at a concentration of 2–50 μg mL^{-1} at 25 °C.

200 nM) were prepared and incubated with NSCs in the presence of a MF ($t = 30$ min) using the previously described optimized method. Untreated NSCs and NSCs treated with MCNP-siRNA constructs were characterized and quantified using immunocytochemistry by staining for oligodendrocytes (myelin binding protein (MBP)) and neuron (β-tubulin (TUJ1)) markers at day 7 after transfection (Figure 4B). From these experiments, we observed a significant increase in the percentage of oligodendrocytes (MBP-positive) and neurons (TUJ1-positive) in the cells treated with si*CAV* or si*SOX9* respectively, versus the spontaneous differentiation condition ($p < 0.01$ for si*CAV* and $p < 0.001$ for si*SOX9* treatment; Figure 4C). Thus, using the magnetically facilitated delivery of MCNP-siRNA constructs, we were able to control the differentiation of NSCs into a particular lineage to a significantly greater extent and within shorter incubation periods than for the untreated control NSCs. Finally, as this is the first report of using MCNPs to deliver genetic materials to NSCs, we investigated the cellular uptake mechanism of our magnetically facilitated delivery of MCNPs into NSCs by treating the NSCs with endocytosis inhibitors and then quantifying their gene silencing effect. From this study, we were able to confirm that the cellular uptake occurred through a combination of clathrin- and caveolae-mediated endocytosis, which is similar to that of standard X-treme-GENE-based and MNP-based transfection (Figure S12).

Finally, to demonstrate the multifunctional advantages that a gold shell can have for MCNP-based delivery of genetic materials and for stem-cell-based therapies, we used dark imaging to confirm the uptake of the MCNPs into NSCs. As our MCNPs possess a thin gold shell and display surface plasmon resonance at 540 nm (Figure 2F), they can be used as cellular imaging modalities with simple dark-field microscopy. In particular, gold nanoparticles are known to scatter visible and infrared light owing to their localized surface plasmons.[21] Furthermore, they are significantly brighter than chemical fluorophores and do not photobleach, thus making them excellent candidates for biological imaging.[22] To this end, we studied the light scattering properties of our MCNPs complexed with control siRNA, by incubating them with NSCs and then monitored their intracellular uptake using a dark-field microscope. As seen in Figure 4D, the MCNPs scatter the incident white light more intensely than the control cells. On the other hand, no noticeable change was seen when the cells were incubated with the magnetic core nanoparticles. Thus, besides improving the solubility and affording facile surface functionalization, the gold shell on our MCNPs can also be used as an imaging modality to confirm the localization of MCNPs to the stem cells before further study or application. Also, owing to the presence of the magnetic core, our MCNPs can afford MRI imaging capability, as can be seen from Figure 4E, thus providing further advantages for in vivo applications.[8] To evaluate whether our MCNPs retain their functions when used as an MRI contrast agent, we carried out MRI studies using MCNPs in phantom agar gels. Increasing the concentration of the MCNPs from 2 $\mu g\,mL^{-1}$ to 50 $\mu g\,mL^{-1}$, led to a significant reduction in T_2, as evident from the decreased signal intensity. Additionally, this decrease was comparable to that of just the core NPs, thus indicating that the Au shell does not negatively affect the MRI contrast of the core. These results, thus demonstrate that our MCNPs could also function as an MRI contrast agent, owing to shortening of T_2 relaxation and higher T_2 relaxivity.

In conclusion, we have synthesized magnetic core–shell nanoparticles (MCNPs) consisting of a highly magnetic $ZnFe_2O_4$ core surrounded by a gold outer shell ($ZnFe_2O_4$@Au), and utilized them for the genetic manipulation of neural stem cells (NSCs) in a highly efficient, biocompatible, and spatiotemporally controlled manner. As a proof-of-concept for the utility of the MCNPS in the genetic manipulation of stem cells, we demonstrated that we could direct the differentiation of NSCs to specific lineages (neurons and oligodendrocytes) using our developed MCNPs to deliver siRNA. In particular, although MCNPs have been utilized for the highly efficient labeling of stem cells, this is the first demonstration of the utilization of MCNPs for the delivery of genetic material (siRNA and pDNA) to stem cells. Moreover, these MCNPs hold a number of advantages for use with stem-cell-based applications owing to multiple functions that result from their composition, a magnetic core with a gold outer-shell. In particular, we have demonstrated that the gold outer-shell: 1) provides a surface for the facile functionalization of our MCNPs with a cationic polyamine-dendrimer, thereby allowing for the complexation of the MCNs with negatively charged genetic materials, 2) enhances biocompatibility of the MCNP with stem cells, and 3) allows for the use of a simple method with which to confirm the presence of MCNPs within stem cells through dark-field imaging. Moreover, previous studies have shown that a gold outer-shell improves aqueous solubility and long-term stability of the MCNPs. On the other hand, we have demonstrated that the magnetic core of the MCNP: 1) retains its excellent magnetic properties, even after the formation of the gold outer-shell, 2) allows us to deliver nanoparticle–biomolecule constructs into the difficult-to-transfect stem cells with high transfection efficiency and with significantly shorter incubation times than for conventional lipid-based transfection agents, and 3) allows for use as an MRI contrast agent, which could be used in the future to track MCNP-transfected stem cells in vivo. Thus, the MCNP-based genetic manipulation method can potentially be a powerful tool for stem cell applications.

Received: March 16, 2013
Published online: May 6, 2013

Keywords: magnetic properties · nanoparticles · neural stem cells · siRNA · stem cell differentiation

[1] a) E. Fuchs, T. Tumbar, G. Guasch, *Cell* **2004**, *116*, 769; b) T. Reya, S. J. Morrison, M. F. Clarke, I. L. Weissman, *Nature* **2001**, *414*, 105; c) J. M. Gimble, A. J. Katz, B. A. Bunnell, *Circ. Res.* **2007**, *100*, 1249; d) G. C. Gurtner, S. Werner, Y. Barrandon, M. T. Longaker, *Nature* **2008**, *453*, 314; e) C. E. Murry, G. Keller, *Cell* **2008**, *132*, 661.

[2] a) U. Lakshmipathy, B. Pelacho, K. Sudo, J. L. Linehan, E. Coucouvanis, D. S. Kaufman, C. M. Verfaillie, *Stem Cells* **2004**, *22*, 531; b) A. Solanki, J. D. Kim, K.-B. Lee, *Nanomedicine* **2008**,

3, 567; c) L. Ferreira, J. M. Karp, L. Nobre, R. Langer, *Cell Stem Cell* **2008**, *3*, 136.
[3] a) X. Y. Zhang, V. F. La Russa, L. Bao, J. Kolls, P. Schwarzenberger, J. Reiser, *Mol. Ther.* **2002**, *5*, 555; b) Y. Ma, A. Ramezani, R. Lewis, R. G. Hawley, J. A. Thomson, *Stem Cells* **2003**, *21*, 111.
[4] D. W. Pack, A. S. Hoffman, S. Pun, P. S. Stayton, *Nat. Rev. Drug Discovery* **2005**, *4*, 581.
[5] a) C. Sapet, N. Laurent, A. de Chevigny, L. Le Gourrierec, E. Bertosio, O. Zelphati, C. Beclin, *Biotechniques* **2011**, *50*, 187; b) L.-Y. Chien, J.-K. Hsiao, S.-C. Hsu, M. Yao, C.-W. Lu, H.-M. Liu, Y.-C. Chen, C.-S. Yang, D.-M. Huang, *Biomaterials* **2011**, *32*, 3275; c) S. I. Jenkins, M. R. Pickard, N. Granger, D. M. Chari, *ACS Nano* **2011**, *5*, 6527.
[6] T. Hyeon, *Chem. Commun.* **2003**, 927.
[7] a) J. K. Park, J. Jung, P. Subramaniam, B. P. Shah, C. Kim, J. K. Lee, J. H. Cho, C. Lee, K. B. Lee, *Small* **2011**, *7*, 1647; b) W. S. Seo, J. H. Lee, X. Sun, Y. Suzuki, D. Mann, Z. Liu, M. Terashima, P. C. Yang, M. V. McConnell, D. G. Nishimura, H. Dai, *Nat. Mater.* **2006**, *5*, 971.
[8] J. T. Jang, H. Nah, J. H. Lee, S. H. Moon, M. G. Kim, J. Cheon, *Angew. Chem.* **2009**, *121*, 1260; *Angew. Chem. Int. Ed.* **2009**, *48*, 1234.
[9] a) L. Y. Wang, H. Y. Park, S. I. I. Lim, M. J. Schadt, D. Mott, J. Luo, X. Wang, C. J. Zhong, *J. Mater. Chem.* **2008**, *18*, 2629; b) C. Tassa, S. Y. Shaw, R. Weissleder, *Acc. Chem. Res.* **2011**, *44*, 842; c) J. Huang, L. H. Bu, J. Xie, K. Chen, Z. Cheng, X. G. Li, X. Y. Chen, *ACS Nano* **2010**, *4*, 7151; d) W. R. Zhao, J. L. Gu, L. X. Zhang, H. R. Chen, J. L. Shi, *J. Am. Chem. Soc.* **2005**, *127*, 8916.
[10] S. Laurent, D. Forge, M. Port, A. Roch, C. Robic, L. V. Elst, R. N. Muller, *Chem. Rev.* **2008**, *108*, 2064.
[11] a) R. Ghosh Chaudhuri, S. Paria, *Chem. Rev.* **2012**, *112*, 2373; b) H. Y. Zhang, M. Y. Lee, M. G. Hogg, J. S. Dordick, S. T. Sharfstein, *ACS Nano* **2010**, *4*, 4733.
[12] a) S. Wang, K.-J. Chen, T.-H. Wu, H. Wang, W.-Y. Lin, M. Ohashi, P.-Y. Chiou, H.-R. Tseng, *Angew. Chem.* **2010**, *122*, 3865; *Angew. Chem. Int. Ed.* **2010**, *49*, 3777; b) Y. D. Jin, C. X. Jia, S. W. Huang, M. O'Donnell, X. H. Gao, *Nat. Commun.* **2010**, *1*, 1.
[13] C. Xu, J. Xie, D. Ho, C. Wang, N. Kohler, E. G. Walsh, J. R. Morgan, Y. E. Chin, S. Sun, *Angew. Chem.* **2008**, *120*, 179; *Angew. Chem. Int. Ed.* **2008**, *47*, 173.
[14] Z. Xu, Y. Hou, S. Sun, *J. Am. Chem. Soc.* **2007**, *129*, 8698.
[15] S. Guo, Y. Huang, Q. Jiang, Y. Sun, L. Deng, Z. Liang, Q. Du, J. Xing, Y. Zhao, P. C. Wang, A. Dong, X.-J. Liang, *ACS Nano* **2010**, *4*, 5505.
[16] a) I. Robinson, L. D. Tung, S. Maenosono, C. Waelti, N. T. K. Thanh, *Nanoscale* **2010**, *2*, 2624; b) Z. H. Ban, Y. A. Barnakov, V. O. Golub, C. J. O'Connor, *J. Mater. Chem.* **2005**, *15*, 4660.
[17] C. Kim, B. P. Shah, P. Subramaniam, K.-B. Lee, *Mol. Pharm.* **2011**, *8*, 1955.
[18] M. R. Pickard, P. Barraud, D. M. Chari, *Biomaterials* **2011**, *32*, 2274.
[19] Y. Li, W.-M. Lau, K.-F. So, Y. Tong, J. Shen, *Neurochem. Int.* **2011**, *59*, 114.
[20] a) M. Wegner, C. C. Stolt, *Trends Neurosci.* **2005**, *28*, 583; b) C. C. Stolt, P. Lommes, E. Sock, M. C. Chaboissier, A. Schedl, M. Wegner, *Genes Dev.* **2003**, *17*, 1677; c) A. Solanki, S. Shah, P. T. Yin, K.-B. Lee, *Sci. Rep.* **2013**, *3*, 1553.
[21] a) M. A. El-Sayed, *Acc. Chem. Res.* **2001**, *34*, 257; b) C. J. Murphy, A. M. Gole, J. W. Stone, P. N. Sisco, A. M. Alkilany, E. C. Goldsmith, S. C. Baxter, *Acc. Chem. Res.* **2008**, *41*, 1721.
[22] P. K. Jain, X. H. Huang, I. H. El-Sayed, M. A. El-Sayed, *Acc. Chem. Res.* **2008**, *41*, 1578.

